catalysts

MDPI

*Article*

# Influence of Surface Chemistry of Carbon Nanofibers on the Hydrodechlorination of Chloroform to Olefins

**Sichen Liu [1,*], Víctor Frutos [1], María Ariadna Álvarez-Montero [1], Luisa María Gómez-Sainero [1], Juan José Rodriguez [1] and Maria Martin-Martinez [2]**

[1] Departamento de Ingeniería Química, Facultad de Ciencias, Campus de Cantoblanco, Universidad Autónoma de Madrid, C/Francisco Tomás y Valiente, 7, 28049 Madrid, Spain
[2] Grupo CyPS, Dto. Ingeniería Química y de Materiales, Universidad Complutense de Madrid, Avda. Complutense s/n, 28040 Madrid, Spain
* Correspondence: sichen.liu@uam.es; Tel.: +34-914975705

**Abstract:** Functionalized carbon nanofibers (CNF) are fascinating materials to be used as supports in Pd-based catalysts for the treatment of waste chloroform (TCM) to produce light olefins through the catalytic hydrodechlorination (HDC). The CNF were functionalized by $HNO_3$, HCl, and urea. Compared to the Pd supported on un-treated CNF, all the catalysts using functionalized CNF as support showed lower turnover frequency values with higher stability, owing to their smaller Pd nanoparticles (NPs). These smaller Pd NPs are formed due to the stronger metal–support interactions promoted by the higher concentration of surface groups on the functionalized catalysts. Since the smaller Pd NPs could hinder the hydrogenation of olefins to paraffins, the selectivity to olefins increased on the functionalized catalysts. Moreover, the N-doped CNF was successfully formed on the catalyst functionalized by urea. Since the nitrogen functional groups (pyridinic N and pyrrolic N) could provide much stronger metal–support interactions compared to the oxygen functional groups on the other catalysts, the catalyst functionalized by urea showed the smallest Pd NPs among the four catalysts, leading to the highest selectivity to light olefins.

**Keywords:** functionalized carbon nanofibers; $HNO_3$; HCl; urea; hydrodechlorination; chloroform; olefins; surface functional groups; N-doped carbon nanofibers



**Citation:** Liu, S.; Frutos, V.; Álvarez-Montero, M.A.; Gómez-Sainero, L.M.; Rodriguez, J.J.; Martin-Martinez, M. Influence of Surface Chemistry of Carbon Nanofibers on the Hydrodechlorination of Chloroform to Olefins. *Catalysts* **2022**, *12*, 1084. https://doi.org/10.3390/catal12101084

Academic Editors: Angela Martins and Ana Paula Carvalho

Received: 31 August 2022
Accepted: 18 September 2022
Published: 21 September 2022



## 1. Introduction

Chloroform (TCM) has been considered a dangerous waste volatile organic compound (VOC) which usually provokes environmental and health problems such as photochemical pollution, global warming, and cancer [1]. Catalytic hydrodechlorination (HDC) is a promising technology which can treat the TCM at moderated operating conditions and produce non-chlorinated products such as methane ($CH_4$), and C2–C3 hydrocarbons. Some previous theorical studies [2,3] suggested that the chloromethanes such as TCM and dichloromethane (DCM) would be firstly fully dechlorinated into non-chlorinated hydrocarbon radicals adsorbed on the surface of active centers, which is energetically favorable. Then, the formed hydrocarbon radicals would be continually hydrogenated into $CH_4$. On the other hand, these formed hydrocarbon radicals could also interact with each other to form C-C bonds leading to the generation of olefins which could be continually hydrogenated into related paraffins [4]. As a structure-sensitive reaction, the selectivity to these products is entirely dependent on the selected metal and catalyst support. Most of the studies reported successfully recovered the TCM to produce $CH_4$ as the main product [5,6]. In some recent works [7,8], interesting results have been obtained for the production of light olefins, such as ethylene ($C_2H_4$) and propylene ($C_3H_6$), from HDC of TCM, which are more valuable for industry. Various noble metals (Pd, Pt, Ru, and Rh) have been studied as the active phase in the HDC of TCM [4], but Pd has demonstrated the highest selectivity to light olefins [4].

Carbon nanofibers (CNF) have attracted enormous interest as catalyst supports in various fields [9], owing to their outstanding mechanical and thermal-stable properties [10]. As a non-microporous material, catalyst deactivation could be resisted since the accumulation of carbon deposits on the catalysts is hindered [11,12]. Moreover, a previous work [7] suggested that mesoporous carbon materials favor the production of light olefins in the HDC of TCM. Since the CNF are a uniform mesoporous carbon material [13], using them as catalyst support would provide highly accessible active centers, promoting the TCM conversion and the formation of light olefins during the HDC of TCM.

The surface functional groups may also influence the olefins' production during the TCM HDC [7]. The presence of surface functional groups usually yields small metal particles through strong metal–support interactions [7]. Small NPs sizes were found to promote the selectivity to olefins [7]. Moreover, the different nature of surface groups may modify the electron density of Pd, which also influences the activity of the catalysts. The modification of the surface chemical properties of CNF has been widely studied by employing different agents such as HCl [14], $HNO_3$ [14,15], urea [16–18], $H_2SO_4$ [19,20], $NH_3$ [19,21,22], and KOH [19]. CNF treated with HCl and $HNO_3$ were employed as catalyst supports in the HDC of 1,2-dichlorobenzene [14] using Pd-based catalysts. The Pd/CNF-HCl provided highly dispersed small Pd NPs, favoring the catalyst activity. CNF-$HNO_3$ generated a higher concentration of surface oxygen groups than CNF-HCl, but lower metal–support interactions [14,15]. Urea is considered a facile and economical nitrogen resource to synthesize N-doped CNF, which, used as catalyst support, could provide strong metal–support interactions and lead to highly stable activity [16]. Thus, the functionalized CNF seems to be an attractive catalyst supports to produce olefins by HDC.

Therefore, in this work, CNF and functionalized CNF will be used as supports of Pd catalysts tested in the HDC of TCM for producing light olefins, analyzing their physicochemical properties through different characterization technologies.

## 2. Results and Discussion

### *2.1. Characterization Results*

The prepared catalysts are denoted as un-treated catalyst (Pd/CNF), catalyst functionalized by HCl (Pd/CNF-Cl), catalyst functionalized by $HNO_3$ (Pd/CNF-N), and catalyst functionalized by urea (Pd/CNF-U). The total-reflection X-ray fluorescence (TXRF) results are shown in Table 1. As can be seen, the four catalysts show similar Pd composition (around 1 wt.%). Their Brunauer–Emmett–Teller (BET) surface areas are also summarized in Table 1. All catalysts present similar surface areas, between 12–13 $m^2\ g^{-1}$. These results suggest that the functionalization treatments do not significantly influence the loaded Pd composition or the surface area of the catalysts.

**Table 1.** Pd composition, BET surface area, mean NP sizes, and dispersion of NPs of the catalysts.

| | Pd/CNF | Pd/CNF-Cl | Pd/CNF-N | Pd/CNF-U |
|---|---|---|---|---|
| Mean NP size (nm) | 3.8 | 2.4 | 2.7 | 1.7 |
| Dispersion of NPs (%) | 29 | 46 | 42 | 67 |
| Loaded Pd (wt.%) | 1.0 | 1.0 | 1.1 | 1.0 |
| BET surface area ($m^2\ g^{-1}$) | 12.3 | 13.0 | 12.3 | 12.5 |

The mean Pd NP sizes were determined by the statistical average employing about 250 NPs sizes obtained from transmission electron microscopy (TEM) images of the catalyst samples. The distributions of these Pd NPs sizes are shown in Figure 1. The mean NP sizes and the dispersion of the NPs are listed in Table 1. The dispersion of Pd NPs is calculated supposing spherical geometry, employing the following equation [8]:

$$Dispersion\ (\%) = \frac{6 \times 10^5 M_w}{\rho_M \cdot \sigma_M \cdot N_A \cdot d} \quad (1)$$

where $M_w$ represents the atomic mass of Pd (106.42 g/mol), $\rho_M$ is the density of Pd (12.02 g/cm$^3$), $\sigma_M$ stands for the Pd effective surface area per atom ($7.87 \times 10^{-20}$ m$^2$), $N_A$ is the number of Avogadro and $d$ corresponds to the mean Pd NP size (in nm), acquired from TEM (Table 1).

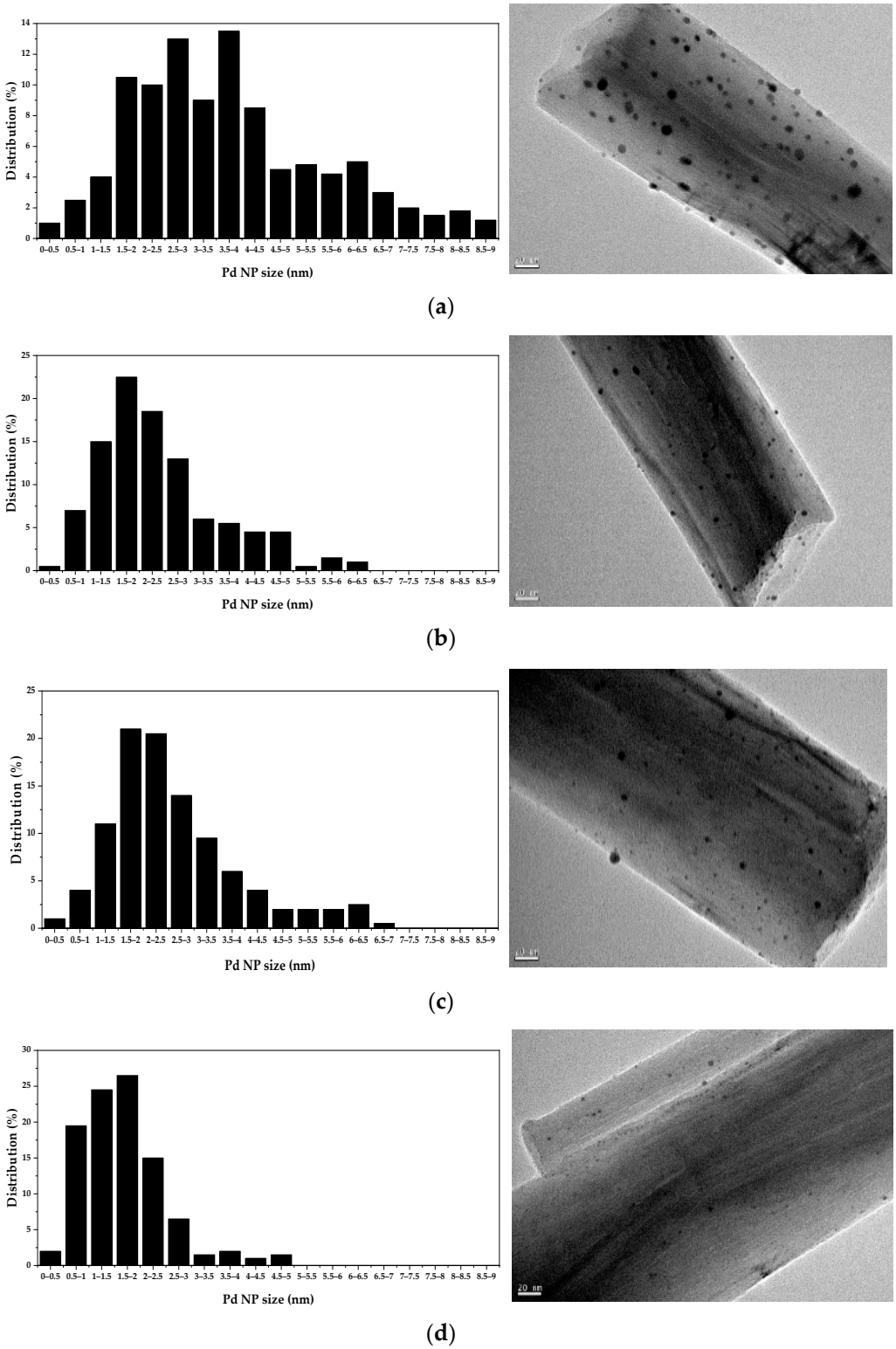


**Figure 1.** Distribution of Pd NP size on different catalysts ((**a**) Pd/CNF; (**b**) Pd/CNF-Cl; (**c**) Pd/CNF-N; (**d**) Pd/CNF-U).

As can be seen, the functionalized catalysts showed smaller NP sizes with higher NPs dispersion than the un-treated catalyst, suggesting the effect of surface functional groups on the metal–support interaction. The mean NP size increases (and NPs dispersion decreases) in the following order: Pd/CNF-U < Pd/CNF-Cl < Pd/CNF-N < Pd/CNF. Among them, Pd/CNF-U shows the smallest mean NP size (1.67 nm), where most NPs are between 0.5–2 nm.

The X-ray diffraction (XRD) patterns of the fresh reduced catalysts are shown in Figure 2. The peaks present at around 26°, 42.5°, 45°, 54°, and 78° are related to the typical crystalline carbon facets usually appearing on structured carbon materials: C(002), C(100), C(101), C(004), and C(110), respectively [23]. The peak at around 40° corresponds to Pd (111) [24]. As can be seen, the intensity of the Pd peak increases in the following order: Pd/CNF-U < Pd/CNF-Cl < Pd/CNF-N < Pd/CNF, as did the mean NP sizes (Table 1). Pd/CNF-U shows two other peaks at around 33° and 36° related to the urea [25]. Probably, the interaction between urea and CNF is forming N-doped CNF.

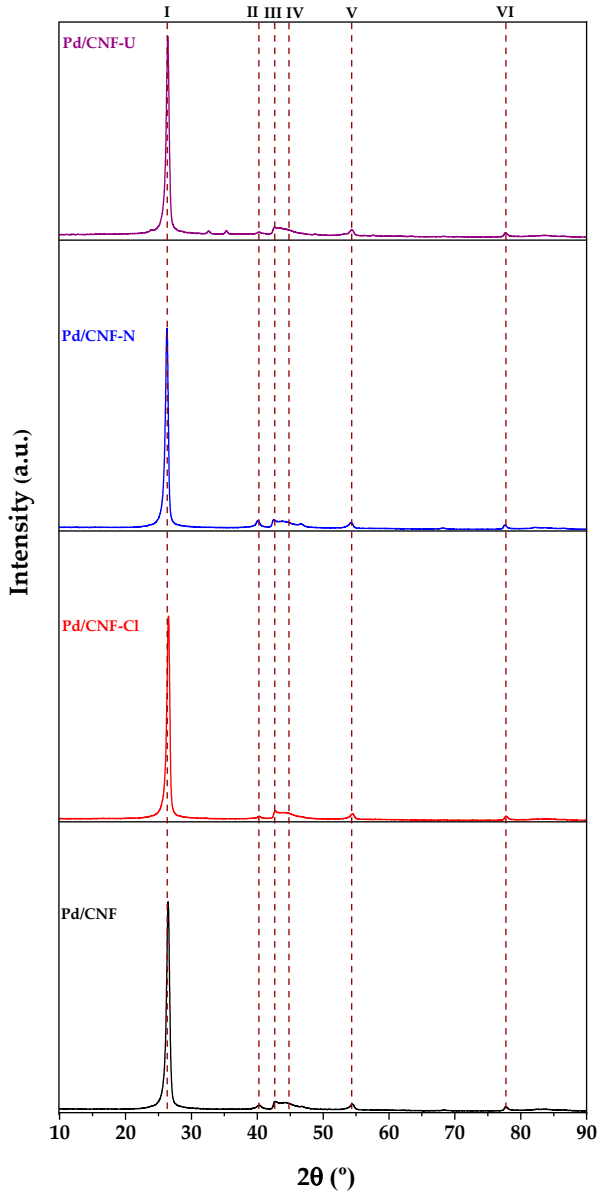


**Figure 2.** XRD patterns of the catalysts (I: C(002); II: Pd(111); III: C(100); IV: C(101); V: C(004); VI: C(110)).

The X-ray photoelectron spectroscopy (XPS) spectra and the deconvoluted species of all fresh reduced catalysts are shown in Figures 3 and 4. The elemental atomic compositions of all species and the relative atomic compositions of O 1s, Pd 3d, and N 1s are summarized in Tables 2–5. In all cases, the O 1s spectrum can be deconvoluted into four species: C=O: 531.1 eV; C-OH: 532.3 eV; C-O-C: 533.5 eV; and COOH: 534.7 eV (Figure 3a). Each Pd 3d spectrum can be deconvoluted into a doublet (Pd $3d_{5/2}$ and Pd $3d_{3/2}$) separated by 5.26 eV. The peaks at around 335.6 eV (and 340.9 eV) are related to the zero-valent Pd ($Pd^0$), the peaks at around 336.7 eV (and 342.0 eV) correspond to PdO, and the peaks at around 338.3 eV (and 343.6 eV) correspond to $PdCl_2$ (Figure 3b). The sum of their values is listed in Table 4 presented as electro-deficient species ($Pd^{n+}$). On Pd/CNF-U, the N 1s spectrum can be deconvoluted into two species: pyridinic N: 398.5 eV; pyrrolic N: 400 eV; [26].

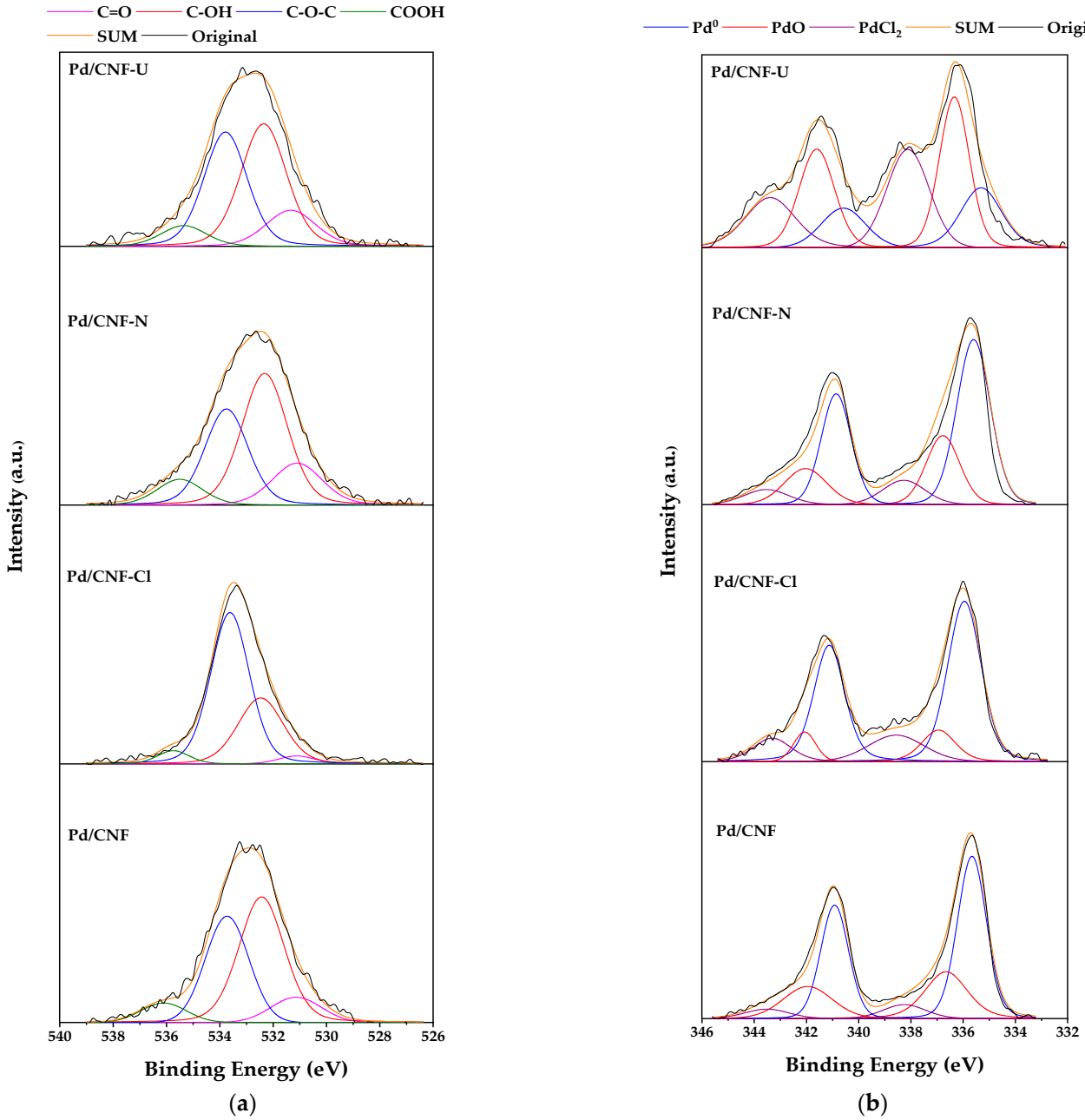


**Figure 3.** XPS profiles of catalysts: (**a**) O 1s; (**b**) Pd 3d.

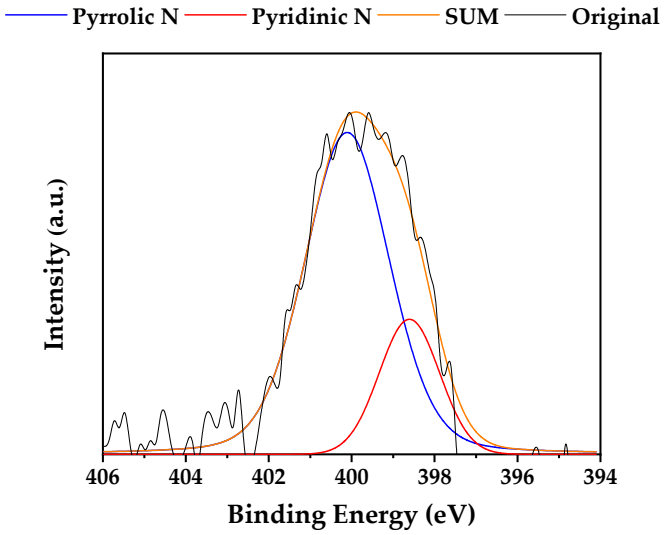


**Figure 4.** XPS profiles of N 1s in Pd/CNF-U.

**Table 2.** XPS elemental atomic composition of supports and catalysts.

| | O 1s (%) | N 1s (%) | Cl 2p (%) | Pd 3d (%) |
|---|---|---|---|---|
| Pd/CNF-U | 4.3 | 1.4 | 0.1 | 0.5 |
| Pd/CNF-N | 4.6 | - | 0.1 | 0.9 |
| Pd/CNF-Cl | 5.9 | - | 0.1 | 0.4 |
| Pd/CNF | 3.6 | - | 0.1 | 0.8 |

**Table 3.** Distribution of oxygen-containing species on the catalysts.

| | O 1s | | | |
|---|---|---|---|---|
| | C = O (%) | C-OH (%) | C-O-C (%) | COOH (%) |
| Pd/CNF-U | 19.7 | 39.5 | 32.5 | 8.4 |
| Pd/CNF-N | 14.8 | 60.8 | 17.3 | 7.1 |
| Pd/CNF-Cl | 4.5 | 30.1 | 61.4 | 4.0 |
| Pd/CNF | 13.4 | 45.6 | 36.4 | 4.6 |

**Table 4.** Distribution of Pd species on the catalysts.

| | Pd 3d | |
|---|---|---|
| | $Pd^0$ (%) | $Pd^{n+}$ (%) |
| Pd/CNF-U | 20.7 | 79.3 |
| Pd/CNF-N | 49.7 | 50.4 |
| Pd/CNF-Cl | 66.8 | 33.3 |
| Pd/CNF | 58.4 | 41.6 |

**Table 5.** Distribution of nitrogen-containing species on Pd/CNF-U.

| | N 1s | |
|---|---|---|
| | Pyridinic N (%) | Pyrrolic N (%) |
| Pd/CNF-U | 21.4 | 78.2 |

The formation of $Pd^0$ seems to be promoted by the presence of electron-donating groups. As can be seen in Table 2, the proportion of oxygen (O 1s %) is higher in the

functionalized catalysts than in the untreated catalyst. Regarding the oxygen functionalities, although different compositions of each species are observed (Table 3), C-OH and C-O-C, are the main oxygen functional groups in all catalysts, which are electron-donating groups, that was found to favor the selectivity to olefins [7]. The catalysts show slight differences in the proportion of electron-donating groups (C-OH + C-O-C), increasing in the order: Pd/CNF-U (72%) < Pd/CNF-N (78.1%) < Pd/CNF (82.0%) < Pd/CNF-Cl (91.5%) in agreement with the increasing order of $Pd^0$ species (Table 4). Among the four catalysts, Pd/CNF-U shows a much lower $Pd^0$ proportion (20.7%) than $Pd^{n+}$ (79.3%) (Table 4), owing to the stronger metal–support interactions given by the presence of nitrogen functional groups, pyridinic N and pyrrolic N on the N-doped CNF (Figure 4 and Table 5). According to a previous DFT study [27], these nitrogen functional groups may strongly interact with Pd atoms.

As the N-doped structured carbon materials usually present outstanding metal–support interactions [9,16,28], they have been employed as supports to synthesize single-atom catalysts [9,27,29,30]. Although the single atomic level is not reached in the active centers on Pd/CNF-U, the strong interactions between pyridinic N and pyrrolic N groups and Pd atoms conduct the smallest Pd NPs among the four catalysts (Table 1 and Figure 1).

Elsewhere, since $PdCl_2$ is used to synthesize all Pd-based catalysts, it is normal to find the presence of chlorine in all the catalysts (Table 2) [31].

### *2.2. Activity Results*

The activity and selectivity results obtained during the HDC of TCM using the four catalysts (Pd/CNF, Pd/CNF-Cl, Pd/CNF-N, and Pd/CNF-U) are shown in Figure 5. The products obtained are: C1 ($CH_4$); C1+ paraffins: ethane ($C_2H_6$), propane ($C_3H_8$), and traces of n-butane (n-$C_4H_{10}$); Olefins: $C_2H_4$, $C_3H_6$, and traces of 1-butene (1-$C_4H_8$); Chloromethanes: monochloromethane (MCM) and DCM. Figure 5a shows the influence of support functionalization on the activity of the catalysts at different reaction temperatures. The functionalized catalysts show considerably lower TCM conversion owing to the formation of the smaller Pd NPs by the interaction with the surface functional groups. As expected, TCM conversion of all catalysts increases when reaction temperature increases. Turnover frequency (TOF) values were calculated at 150 °C. The relationship between the TOF values of catalysts and their mean Pd NP sizes is shown in Figure 6. TOF values decrease in the following order Pd/CNF (12 $h^{-1}$) > Pd/CNF-N (5 $h^{-1}$) > Pd/CNF-Cl (3 $h^{-1}$) > Pd/CNF-U (1 $h^{-1}$), as Pd NP sizes decrease, similar results were observed in some previous studies using Pd-based catalysts in the HDC of chloromethanes [8,32].

As seen in Figure 5, the higher temperature increases TCM conversion and selectivity to olefins, which was also observed in some previous works [4,7]. Therefore, the highest temperature (250 °C) was selected to show the selectivities to the main products (Figure 5b). Selectivity to olefins increases in the following order: Pd/CNF (ca. 25%) < Pd/CNF-Cl (ca. 31%) < Pd/CNF-N (ca. 50%) < Pd/CNF-U (ca. 70%). On the contrary, selectivity to $CH_4$ decreases in the same order. In contrast with most of Pd carbon supported catalysts used in previous studies [1,7,31], Pd/CNF supported catalysts show a considerable selectivity to olefins at mild reaction temperature which can be ascribed to the high proportion of electron-donating surface groups. However, the functionalized catalysts show higher and more stable selectivity to olefins compared to the un-treated catalyst (Figure 7), promoted by their smaller Pd NPs, formed by the interaction with the surface functional groups (Figures 1 and 2, Table 1), smaller Pd NPs, hinder the olefins' hydrogenation into paraffins, as observed in a previous work [7]. A previous simulation study [3] indicated that, over the Pd surface, the TCM would be fully dechlorinated into a CH* radical. Then, the CH* would be hydrogenated into $CH_2$* and $CH_3$* radicals, and $CH_4$. It seems that smaller Pd NPs on the functionalized catalysts show lower hydrogenation ability than the bigger NPs of the un-treated catalyst, occurring the hydrogenation of CH* to a lesser degree. The formation of the C-C bond might be favored over the Pd surface on the functionalized catalysts, promoting the formation of C1+ hydrocarbons, especially olefins due to the lack of

hydrogen, since the olefins were be found to be an intermediate in the hydrodechlorination of chloromethanes to C2 hydrocarbons, which could be continually hydrogenated into paraffins [4]. Among the functionalized catalysts, the Pd/CNF-U presents the highest selectivity to olefins (ca. 70%, Figure 7d) owing to its smallest NPs size formed by the interaction with pyridinic N and pyrrolic N groups (Table 1, Figure 4). Herein, nitrogen functional groups present a strong metal–support interaction, hindering the growth of Pd NPs, leading to the formation of the smallest Pd NPs and promoting the highest selectivity to olefins among the four catalysts.

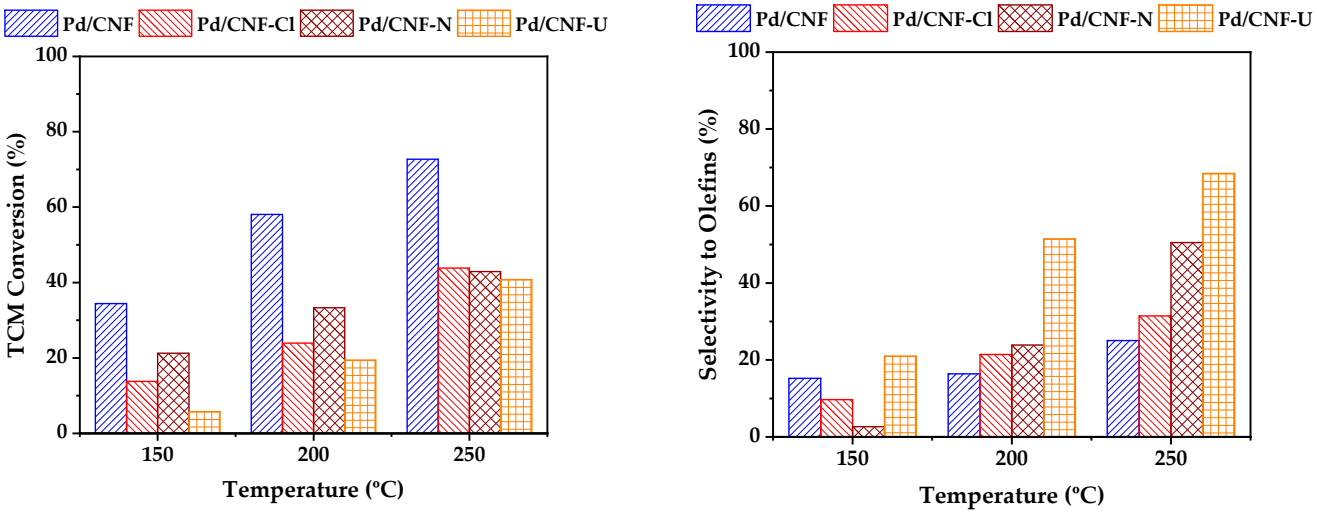


**Figure 5.** Influence of surface functionalization at different reaction temperature on (**a**) TCM conversion and (**b**) selectivity to olefins (space-time (τ) = 0.2 kg h mol$^{-1}$; $H_2$/TCM = 50).

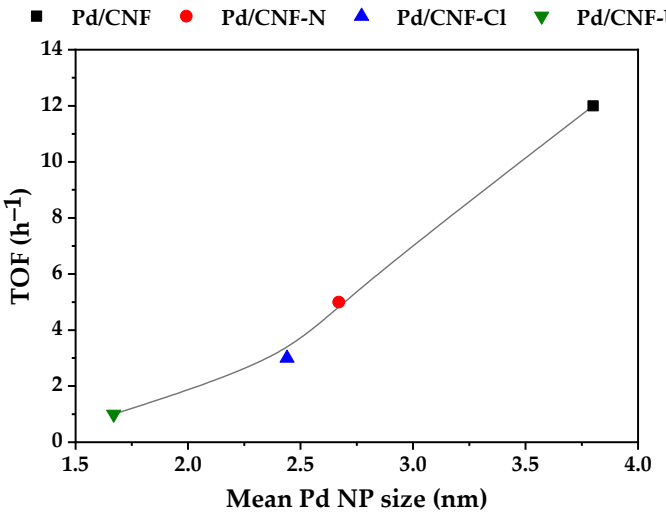


**Figure 6.** TOF (150 °C) versus mean Pd NP sizes values of the catalysts.

Figure 7 also shows the stability of the catalysts at 250 °C. The un-treated catalyst shows the highest initial TCM conversion (ca. 70%, Figure 7a), but its deactivation is evident. On the contrary, the three functionalized catalysts show a similar lower TCM conversion (ca. 40%) and no significant deactivation, suggesting that although their smaller Pd NPs may not present high activity (Table 1), they may promote higher catalyst stability in the HDC of TCM, as it was also observed in a previous study [7,31].

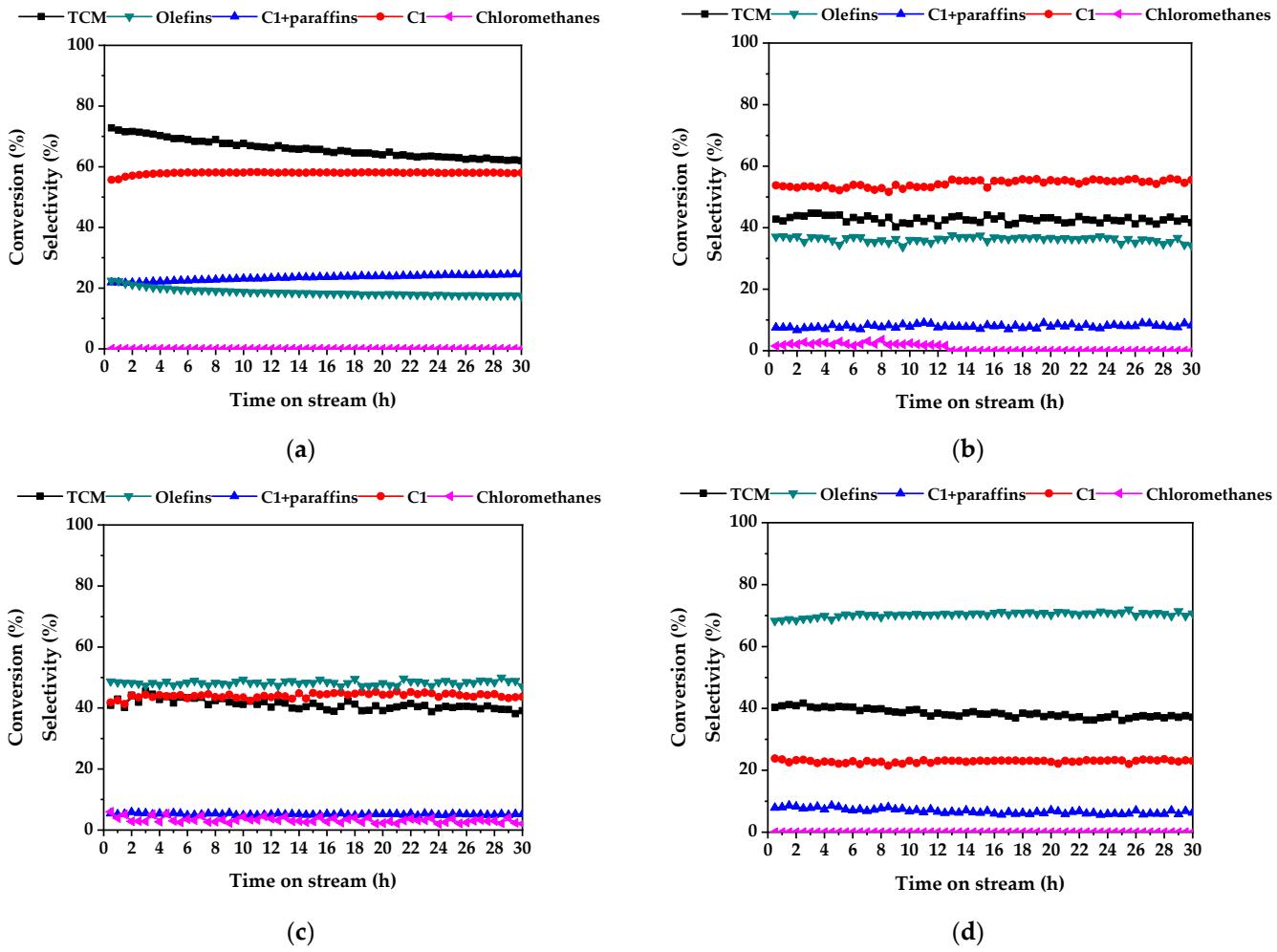


**Figure 7.** Stability of catalysts during the HDC of TCM: (**a**) Pd/CNF, (**b**) Pd/CNF-Cl, (**c**) Pd/CNF-N, (**d**) Pd/CNF-U ($T_{reaction}$ = 250 °C; τ = 0.2 kg h $mol^{-1}$; $H_2$/TCM = 50).

## 3. Materials and Methods

### *3.1. Functionalization of CNF*

Commercial CNF (Sigma-Aldrich, St. Louis, MO, USA, diameter ≈ 100 nm, length ≈ 20–200 μm) have been functionalized by: (i) physical mixture of CNF with urea (proportion 7:3 in weight), ball-milled in a Orto-Alresa de 250 RPM for 4 h at a vibration frequency of 1.5 rounds $s^{-1}$, followed by thermal treatment at 600 °C under $N_2$ flow for 1 h, as described by Soares et al. [33]; (ii) oxidation with $HNO_3$, adapting the procedure used by Rocha et al. [34], stirring a mixture of 7.5 g $L^{-1}$ of CNF and $HNO_3$ (7 mol $L^{-1}$) in a round flask at boiling temperature for 3 h; and treatment with HCl, sonicating for 20 min a mixture of 13.3 g $L^{-1}$ of CNF and concentrated HCl (37%), followed by overnight stirring, as described by Yang et al. [35]. The solids functionalized with $HNO_3$ and HCl were washed with distilled water until neutral pH and dried at 110 °C overnight.

### *3.2. Preparation of Catalysts*

These solids have been used as supports for the synthesis of 1 wt.% Pd/CNF catalysts, prepared by incipient wetness impregnation, employing $PdCl_2$ (>99%, Sigma-Aldrich) dissolved in an acidic aqueous solution as Pd precursor. The catalysts were dried at 100 °C with a heating rate of 20 °C $h^{-1}$ for 2 h. Finally, the dried catalysts were activated through a reduction process under a 50 $Ncm^3$ $min^{-1}$ $H_2$ flow (>99.999%, supplied by Nippon Gases) at 250 °C for 2 h.

### 3.3. Characterization

The porous structure of the catalysts was analyzed by $N_2$ adsorption–desorption at—196 °C employing a Micromeritics equipment (Tristar II 3020). The catalyst samples were previously outgassed at 150 °C overnight. The BET equation was used to calculate the specific surface areas. The loaded Pd concentration was analyzed by TXRF. A TXRF 8030C spectrometer (Cameca, Gennevilliers, France) is used together with a 3 kW X-ray tube with a Mo/W alloy anode connected to a double-W/C multilayer monochromator. A Si(Li) detector (Oxford Instruments, Abingdon, UK) was employed with an active area of 80 $mm^2$. The resolution of this detector was 150 eV at 5.9 keV. The catalyst samples were analyzed at 50 kV with an auto-adjusted intensity for achieving nearly 8500 cps with a signals-collection frequency of 500 s/signal. The Pd NP sizes were measured through the TEM images obtained from a JEOL JEM-2100F microscope, which operated at 200 kV with a resolution of 0.19 nm. The mean Pd NP size of each catalyst was calculated through measurements of about 250 NP. The crystalline structure of the catalysts was measured through XRD analysis in an X'Pert PRO PANalytical diffractometer with a θ-θ configuration. The samples were scanned by CuKα radiation (λ = 1.5406 Å, 45 kV, 40 mA). The scan range (2θ) was 4–90° with a step size of 0.04 and a counting time of 20 s. The catalysts' surface composition and oxidation state were analyzed by XPS using a Multitechnique System of Physical Electronics 5700 C with a MgKα radiation equal to 1253.6 eV. The composition was analyzed by a broad spectrum obtained through binding energy (BE) up to 1200 eV. C1s peak (284.6 eV) was used as an internal standard to correct the changes in BE caused by sample charging. After smooth Shirley background subtraction, the deconvolution of XPS spectra was realized using mixed Gaussian–Lorentzian functions with a least-squares method. The relative atomic composition of elements was related to the area of deconvoluted peaks obtained from related core-level curves applying Wagner sensitivity factors [36].

### 3.4. Catalytic Activity Tests

The activity of the catalysts in the HDC of TCM was tested in a continuous flow Microactivity (PID Eng&Tech, São Paulo, Brazil) reaction system described elsewhere [37], consisting of a quartz fixed-bed microreactor (internal diameter 9 nm), connected to a gas-chromatograph (Agilent 7820A) equipped with a capillary column (CP-SilicaPLOT, 60 m × 0.53 mm ID, Agilent, Madrid, Spain), using a Flame Ionization Detector (FID) to measure the concentration of TCM and products. The experiments were performed at atmospheric pressure, with a total flow rate of 100 $Ncm^3\ min^{-1}$, a TCM inlet concentration of 1000 ppmv, an $H_2$/TCM molar ratio of 50:1, and a τ = 0.2 kg h $mol^{-1}$. Various reaction temperatures were tested: 150 °C, 175 °C, 200 °C, 225 °C, and 250 °C.

The performance of the catalysts in the HDC of TCM reaction was measured in terms of TCM conversion (*X(TCM)*) and selectivities to different products (*S(i)*):

$$X(TCM) = \frac{C(TCM)_{inlet} - C(TCM)_{outlet}}{C(TCM)_{inlet}} \times 100\% \quad (2)$$

$$S(i) = \frac{C(i)_{outlet} \times N(Carbon)_i}{C(i)_{outlet} \times N(Carbon)_i + C(j)_{outlet} \times N(Carbon)_j + \cdots} \times 100\% \quad (3)$$

where $C(TCM)_{inlet}$ and $C(TCM)_{outlet}$ refer to TCM concentration at the inlet and outlet of the microreactor, respectively, $C(i)_{outlet}$ and $C(j)_{outlet}$ refer to the concentrations of the products *i* and *j*, respectively, at the outlet of the microreactor, and *N(Carbon)i* and *N(Carbon)j* are carbon atoms number in the products *i* and *j*, respectively.

The TOF was calculated as the number of TCM molecules converted per number of accessible Pd atoms and time. The number of accessible Pd atoms is calculated using the nominal Pd content (μmol $g^{-1}$) of the catalysts multiplied by the dispersion value (Table 1).

## 4. Conclusions

The CNF supported catalysts tested promote olefins formation in the HDC of TCM when compared to other carbonaceous materials supported Pd catalysts because of their high amount of electron-donating surface groups. Moreover, the surface chemistry of the functionalized catalysts has a great influence in the production of olefins by HDC of TCM through the reduction in Pd NPs size. Compared to the un-treated CNF, the functionalized catalysts show higher concentrations of surface functional groups, which promote the formation of smaller Pd NPs due to a stronger metal–support interaction. The functionalized catalysts, with smaller Pd NPs, demonstrate lower TOF but higher selectivity to olefins and stability than the un-treated catalyst. Smaller Pd NPs present lower hydrogenation ability of reaction intermediates and hinder the hydrogenation of adsorbed olefins into paraffins.

N-dopped CNF is successfully synthesized using urea. Since the interactions between the nitrogen functional groups (pyridinic N and pyrrolic N) and Pd atoms are much stronger than that given by oxygen functional groups, the smallest Pd NPs are formed on Pd/CNF-U among the four catalysts, leading to its highest selectivity to olefins.

**Author Contributions:** Conceptualization, V.F., M.A.Á.-M. and M.M.-M.; methodology, S.L. and V.F.; investigation, S.L., V.F., M.A.Á.-M. and M.M.-M.; writing—original draft preparation, S.L.; writing—review and editing, M.A.Á.-M., L.M.G.-S., J.J.R. and M.M.-M.; supervision, M.M.-M., J.J.R. and L.M.G.-S.; project administration, M.M.-M. and L.M.G.-S.; funding acquisition, M.M.-M. and L.M.G.-S. All authors have read and agreed to the published version of the manuscript.

**Funding:** This research was funded by FEDER/Ministerio de Ciencia, Innovación y Universidades—Agencia Estatal de Investigación (CTM2017-85498-R) and Comunidad de Madrid/UAM (SI1/PJI/2019-00487).

**Data Availability Statement:** Not applicable.

**Acknowledgments:** The authors acknowledge FEDER/Ministerio de Ciencia, Innovación y Universidades—Agencia Estatal de Investigación (CTM2017-85498-R) and Comunidad de Madrid/UAM (SI1/PJI/2019-00487) for financial support. Maria Martin-Martinez acknowledges a postdoctoral grant (2017-T2/AMB-5668), from the Comunidad de Madrid "Atracción de Talento" programme. Sichen Liu acknowledges Ministerio de Ciencia e Innovación for his research grant (PRE2018-084424).

**Conflicts of Interest:** The authors declare no conflict of interest. The funders had no role in the design of the study; in the collection, analyses, or interpretation of data; in the writing of the manuscript, or in the decision to publish the results.

## References

1. Liu, S.; Otero, J.A.; Martin-Martinez, M.; Rodriguez-Franco, D.; Rodriguez, J.J.; Gómez-Sainero, L.M. Understanding Hydrodechlorination of Chloromethanes. Past and Future of the Technology. *Catalysts* **2020**, *10*, 1462. [CrossRef]
2. Omar, S.; Palomar, J.; Gómez-Sainero, L.M.; Álvarez-Montero, M.A.; Maria Martin-Martinez, M.; Rodriguez, J.J. Density Functional Theory Analysis of Dichloromethane and Hydrogen Interaction with Pd Clusters: First Step to Simulate Catalytic Hydrodechlorination. *J. Phys. Chem. C* **2011**, *115*, 14180–14192. [CrossRef]
3. Xu, L.; Bhandar, S.; Chen, J.; Glasgow, J.; Mavrikakis, M. Chloroform Hydrodechlorination on Palladium Surfaces: A Comparative DFT Study on Pd(111), Pd(100), and Pd(211). *Top. Catal.* **2020**, *63*, 762–776. [CrossRef]
4. Gómez-Sainero, L.M.; Palomar, J.; Omar, S.; Fernández, C.; Bedia, J.; Álvarez-Montero, A.; Rodriguez, J.J. Valorization of chloromethanes by hydrodechlorination with metallic catalysts. *Catal. Today* **2018**, *310*, 75–85. [CrossRef]
5. Velázquez, J.C.; Leekumjorn, S.; Nguyen, Q.X.; Fang, Y.-L.; Heck, K.N.; Hopkins, G.D.; Reinhard, M.; Wong, M.S. Chloroform Hydrodechlorination Behavior of Alumina-supported Pd and PdAu Catalysts. *AIChE J.* **2013**, *59*, 4474–4482. [CrossRef]
6. Bedia, J.; Arevalo-Bastante, A.; Grau, J.M.; Dosso, L.A.; Rodriguez, J.J.; Mayoral, A.; Diaz, I.; Gómez-Sainero, L.M. Effect of the Pt–Pd molar ratio in bimetallic catalysts supported on sulfated zirconia on the gas-phase hydrodechlorination of chloromethanes. *J. Catal.* **2017**, *352*, 562–571. [CrossRef]
7. Fernandez-Ruiz, C.; Bedia, J.; Andreoli, S.; Eser, S.; Rodríguez, J.J.; Gómez-Sainero, L. Selectivity to Olefins in the Hydrodechlorination of Chloroform with Activated Carbon Supported Palladium Catalysts. *Ind. Eng. Chem. Res.* **2019**, *58*, 20592–20600. [CrossRef]

8. Fernandez-Ruiz, C.; Bedia, J.; Grau, J.M.; Romero, A.C.; Rodríguez, D.; Rodríguez, J.J.; Gómez-Sainero, L.M. Promoting Light Hydrocarbons Yield by Catalytic Hydrodechlorination of Residual Chloromethanes Using Palladium Supported on Zeolite Catalysts. *Catalysts* **2020**, *10*, 199. [CrossRef]
9. Gerber, I.C.; Serp, P. A Theory/Experience Description of Support Effects in Carbon-Supported Catalysts. *Chem. Rev.* **2020**, *120*, 1250–1349. [CrossRef]
10. De Jong, K.P.; Geus, J.W. Carbon Nanofibers: Catalytic Synthesis and Applications. *Catal. Rev.-Sci. Eng.* **2000**, *42*, 481–510. [CrossRef]
11. Amorim, C.; Yuan, G.; Patterson, P.M.; Keane, M.A. Catalytic hydrodechlorination over Pd supported on amorphous and structured carbon. *J. Catal.* **2005**, *234*, 268–281. [CrossRef]
12. Bueres, R.F.; Asedegbega-Nieto, E.; Díaz, E.; Ordóñez, S.; Díez, F.V. Preparation of carbon nanofibres supported palladium catalysts for hydrodechlorination reactions. *Catal. Commun.* **2008**, *9*, 2080–2084. [CrossRef]
13. Díaz, E.; Ordóñez, S.; Vega, A. Adsorption of volatile organic compounds onto carbon nanotubes, carbon nanofibers, and high-surface-area graphites. *J. Coll. Interf. Sci.* **2007**, *305*, 7–16. [CrossRef]
14. Netskina, O.V.; Komova, O.V.; Tayban, E.S.; Oderova, G.V.; Mukha, S.A.; Kuvshinov, G.G.; Simagina, V.I. The influence of acid treatment of carbon nanofibers on the activity of palladium catalysts in the liquid-phase hydrodechlorination of dichloro-benzene. *App. Catal. A: Gen.* **2013**, *467*, 386–393. [CrossRef]
15. Din, I.U.; Shaharun, M.S.; Subbarao, D.; Naeem, A. Surface modification of carbon nanofibers by $HNO_3$ treatment. *Ceram. Intern.* **2016**, *42*, 966–970. [CrossRef]
16. Liu, D.; Zhang, X.; You, T. Urea-treated carbon nanofibers as efficient catalytic materials for oxygen reduction reaction. *J. Power Sources* **2015**, *273*, 810–815. [CrossRef]
17. Zou, K.; Deng, Y.; Chen, J.; Qian, Y.; Yang, Y.; Li, Y.; Chen, G. Hierarchically porous nitrogen-doped carbon derived from the activation of agriculture waste by potassium hydroxide and urea for high-performance supercapacitors. *J. Power Sources* **2018**, *378*, 579–588. [CrossRef]
18. Zhang, W.; Huang, Y.; Yuan, F.; Sun, B.; Lin, J.; Yang, J.; Sun, D. Nitrogen-doped Carbon Nanofibers Network Derived from Bacterial Cellulose for the Oxygen Reduction Reaction. *Chem. Lett.* **2019**, *48*, 1188–1191. [CrossRef]
19. Yin, J.; Qiu, Y.; Yu, J.; Zhou, X.; Wu, W. Enhancement of electrocatalytic activity for oxygen reduction reaction in alkaline and acid media from electrospun nitrogen-doped carbon nanofibers by surface modification. *RSC Adv.* **2013**, *3*, 15655–15663. [CrossRef]
20. Klein, K.L.; Melechko, A.V.; McKnight, T.E.; Retterer, S.T.; Rack, P.D.; Fowlkes, J.D.; Joy, D.C.; Simpson, M.L. Surface characterization and functionalization of carbon nanofibers. *J. Appl. Phys.* **2008**, *103*, 061301. [CrossRef]
21. Wang, M.-X.; Guo, Z.; Huang, Z.-H.; Kang, F. NH3-activated carbon nanofibers for low-concentration NO removal at room temperature. *Catal. Commun.* **2015**, *62*, 83–88. [CrossRef]
22. Tian, X.; Zhao, N.; Song, Y.; Wang, K.; Xu, D.; Li, X.; Guo, Q.; Liu, L. Synthesis of nitrogen-doped electrospun carbon nanofibers with superior performance as efficient supercapacitor electrodes in alkaline solution. *Electrochim. Acta* **2015**, *185*, 40–51. [CrossRef]
23. Li, Z.Q.; Lu, C.J.; Xia, Z.P.; Zhou, Y.; Luo, Z. X-ray diffraction patterns of graphite and turbostratic carbon. *Carbon* **2007**, *45*, 1686–1695. [CrossRef]
24. Kern, A.; Eysel, W. *ICDD Grant-in-Aid*; Mineralogisch-Petrograph Institut, Universität Heidelberg: Heidelberg, Germany, 1993.
25. Fang, S.; Ma, H.; Guo, L.; Chen, L.; Yao Wang, Y.; Ding, L.; Cai, Z.; Wang, J.; Jia, X. Characteristics of urea under high pressure and high temperature. *Chin. Phys. B* **2019**, *28*, 098101. [CrossRef]
26. Huang, R.; Cao, C.; Liu, J.; Sun, D.; Song, W. N-Doped carbon nanofibers derived from bacterial cellulose as an excellent metal-free catalyst for selective oxidation of arylalkanes. *Chem. Commun.* **2019**, *55*, 1935. [CrossRef]
27. Bulushev, D.A.; Zacharska, M.; Lisitsyn, A.S.; Podyacheva, Q.Y.; Hage, F.S.; Ramasse, Q.M.; Bangert, U.; Bulusheva, L.G. Single Atoms of Pt-Group Metals Stabilized by N-Doped Carbon Nanofibers for Efficient Hydrogen Production from Formic Acid. *ACS Catal.* **2016**, *6*, 3442–3451. [CrossRef]
28. Matter, P.H.; Zhang, L.; Ozkan, U.S. The role of nanostructure in nitrogen-containing carbon catalysts for the oxygen reduction reaction. *J. Catal.* **2006**, *239*, 83–96. [CrossRef]
29. Gao, X.; Zhou, Y.; Liu, S.; Cheng, Z.; Tan, Y.; Shen, Z. Single cobalt atom anchored on N-doped graphyne for boosting the overall water splitting. *App. Surf. Sci.* **2020**, *502*, 144155. [CrossRef]
30. Qi, J.; Xua, Q.; Zhou, D.; Yin, J.; Jiang, Q. Preparation of Cu single atoms on N-doped carbon materials with supercritical $CO_2$ deposition. *J. Supercrit. Fluids* **2021**, *171*, 105202. [CrossRef]
31. Martin-Martinez, M.; Álvarez-Montero, A.; Gómez-Sainero, L.M.; Baker, R.T.; Palomar, J.; Omar, S.; Eser, S.; Rodriguez, J.J. Deactivation behavior of Pd/C and Pt/C catalysts in the gas-phasehydrodechlorination of chloromethanes: Structure–reactivity relationship. *Appl. Catal. B: Environ.* **2015**, *162*, 532–543. [CrossRef]
32. Bonarowska, M.; Kaszkur, Z.; Kepinski, L.; Karpinski, Z. Hydrodechlorination of tetrachloromethane on alumina- and silica-supported platinum catalysts. *Appl. Catal. B Environ.* **2010**, *99*, 248–256. [CrossRef]
33. Soares, O.S.G.P.; Rocha, R.P.; Gonçalves, A.G.; Figueiredo, J.L.; Órfão, J.J.M.; Pereira, M.F.R. Easy method to prepare N-doped carbon nanotubes by ball milling. *Carbon* **2015**, *91*, 114–121. [CrossRef]
34. Rocha, R.P.; Sousa, J.P.S.; Silva, A.M.T.; Pereira, M.F.R.; Figueiredo, J.L. Catalytic activity and stability of multiwalled carbon nanotubes in catalytic wet air oxidation of oxalic acid: The role of the basic nature induced by the surface chemistry. *Appl. Catal. B Environ.* **2011**, *104*, 330–336. [CrossRef]

35. Yang, S.; Li, X.; Zhu, W.; Wang, J.; Descorme, C. Catalytic activity, stability and structure of multi-walled carbon nanotubes in the wet air oxidation of phenol. *Carbon* **2008**, *46*, 445–452. [CrossRef]
36. Wagner, C.D.; Davis, L.E.; Zeller, M.V.; Taylor, J.A.; Raymond, R.H.; Gale, L.H. Empirical atomic sensitivity factors for quantitative analysis by electron spectroscopy for chemical analysis. *Surf. Interface Anal.* **1981**, *3*, 211–225. [CrossRef]
37. De Pedro, Z.M.; Gómez-Sainero, L.M.; Gonzalez-Serrano, E.; Rodríguez, J.J. Gas-Phase hydrodechlorination of dichloro-methane at low concentrations with palladium/carbon catalysts. *Ind. Eng. Chem. Res.* **2006**, *45*, 7760–7766. [CrossRef]